Time-dependent Radiation Transfer in Internal Shock Model for Blazar Jets

Authors: Manasvita Joshi and Markus Böttcher (Ohio University)

Abstract – We use the internal shock model to explore the acceleration of particles and the subsequent production of radiation via synchrotron and synchrotron self Compton (SSC) processes at sub-pc scales inside a relativistic jet. A single inelastic collision is assumed to take place between an inner fast shell and an outer slow shell. We consider the instantaneous acceleration of relativistic particles at the forward and reverse shocks and treat the subsequent radiation transfer self-consistently by taking into account the inhomogeneity in the photon density throughout the emission region and the light-travel time effects. Here, we present simulated spectral energy distributions (SED) obtained from carrying out this analysis.

Introduction – Blazar jets are highly violent in nature and are dominated by ultrarelativistic particles. The SED of blazars consists of two spectral bumps. The low-energy component is due to synchrotron radiation emanating from relativistic particles, and the high-energy component (for leptonic jet model) is a result of Compton upscattering of the seed photon field by ultrarelativistic particles. The mode of acceleration of plasma electrons (and positrons) to highly relativistic energies and its location in the jet is still not completely understood. One such method to comprehend the physics of acceleration is the internal shock model, in which the central engine (black hole + accretion disk) spews out shells of plasma with varied velocity, mass, and energy. The collision between such shells gives rise to internal shocks (reverse (RS) and forward (FS)), which convert the ordered bulk kinetic energy of the plasma into the magnetic field energy and the random kinetic energy of the particles. The highly accelerated particles then start to radiate and produce the emission observed from the jet.

Internal Shock Model – We consider a single inelastic collision between a slower moving outer shell and a faster moving inner shell. The two shocks, RS and FS, that result from the collision are separated by a contact discontinuity (CD) across which the pressure and velocity of the shocked fluids stay constant. As the two shocks start to propagate into their respective shells, they accelerate particles, which then lose their energy to produce the observed emission. A schematic of the model is shown in Figure 1. The dynamics of the collision has been treated hydrodynamically based on the approach of [4]. The bulk Lorentz factor (BLF), Γ_{sh} , of the emission region is obtained from the condition of equal pressure for the shocked fluids across the CD. The Γ_{sh} yields the value of the magnetic field, B, and the minimum random Lorentz factor (RLF), γ_{min} , of the particles [4]. The maximum RLF, γ_{max} , [2] and the normalization factor of the injection function are also obtained from the shock dynamics [3]. These emission region parameters are then used to calculate the radiative energy loss rates, photon emissivities, and the temporal evolution of electron population [1]. All the BLFs are in the lab frame whereas all the other parameters are in the comoving frame of the emission region.
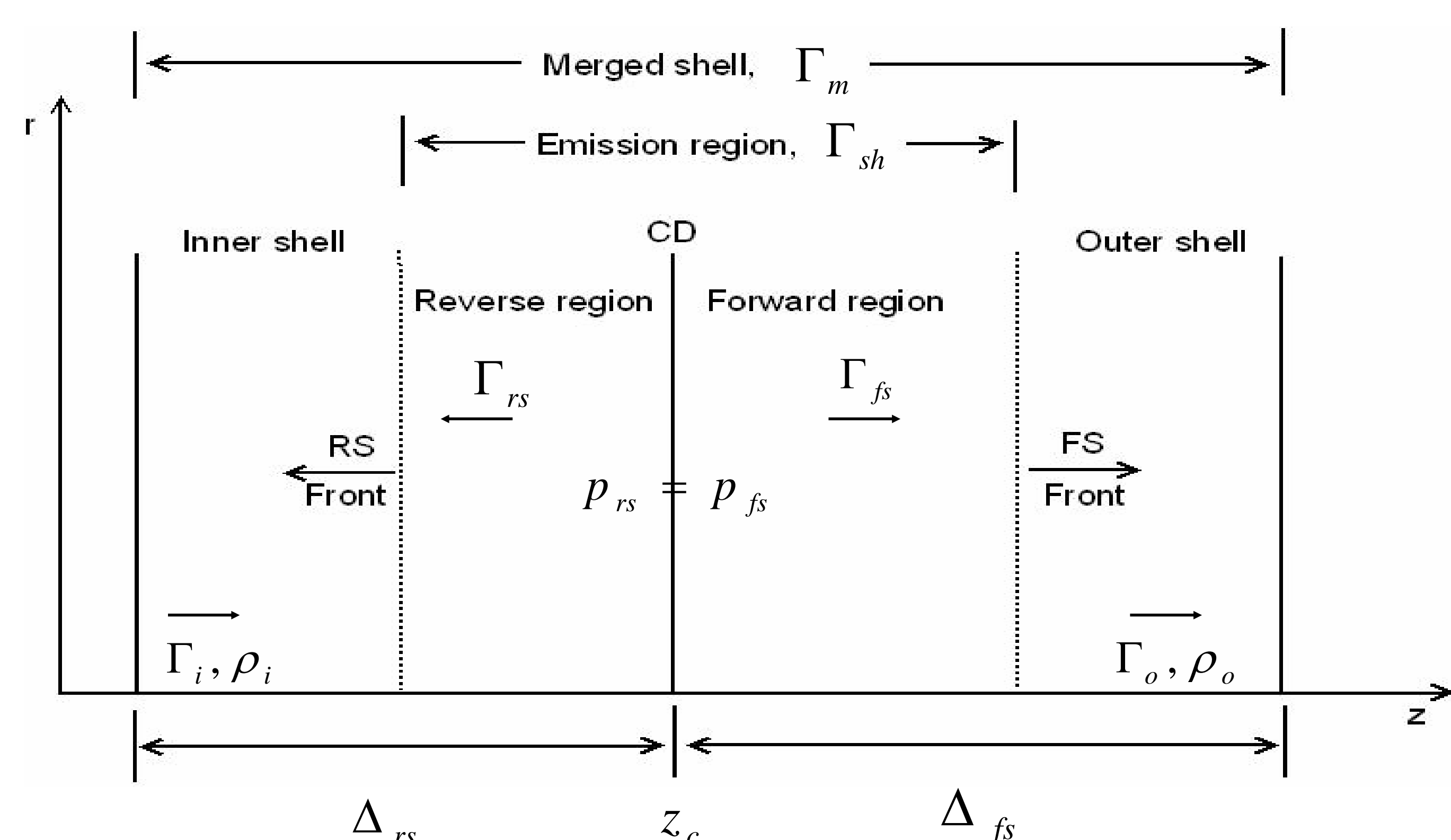

Fig. 1: Schematic of the emission region with RS traveling into the inner shell of BLF, Γ_i , and FS moving into the outer shell with BLF, Γ_o ($\Gamma_i > \Gamma_o$). The pressures of the two shocked fluids, p_{rs} & p_{fs} are the same across the CD. Δ_{rs} & Δ_{fs} are the widths of the inner and outer shell after the collision in the lab frame (central engine frame) obtained from the shock dynamics [1].
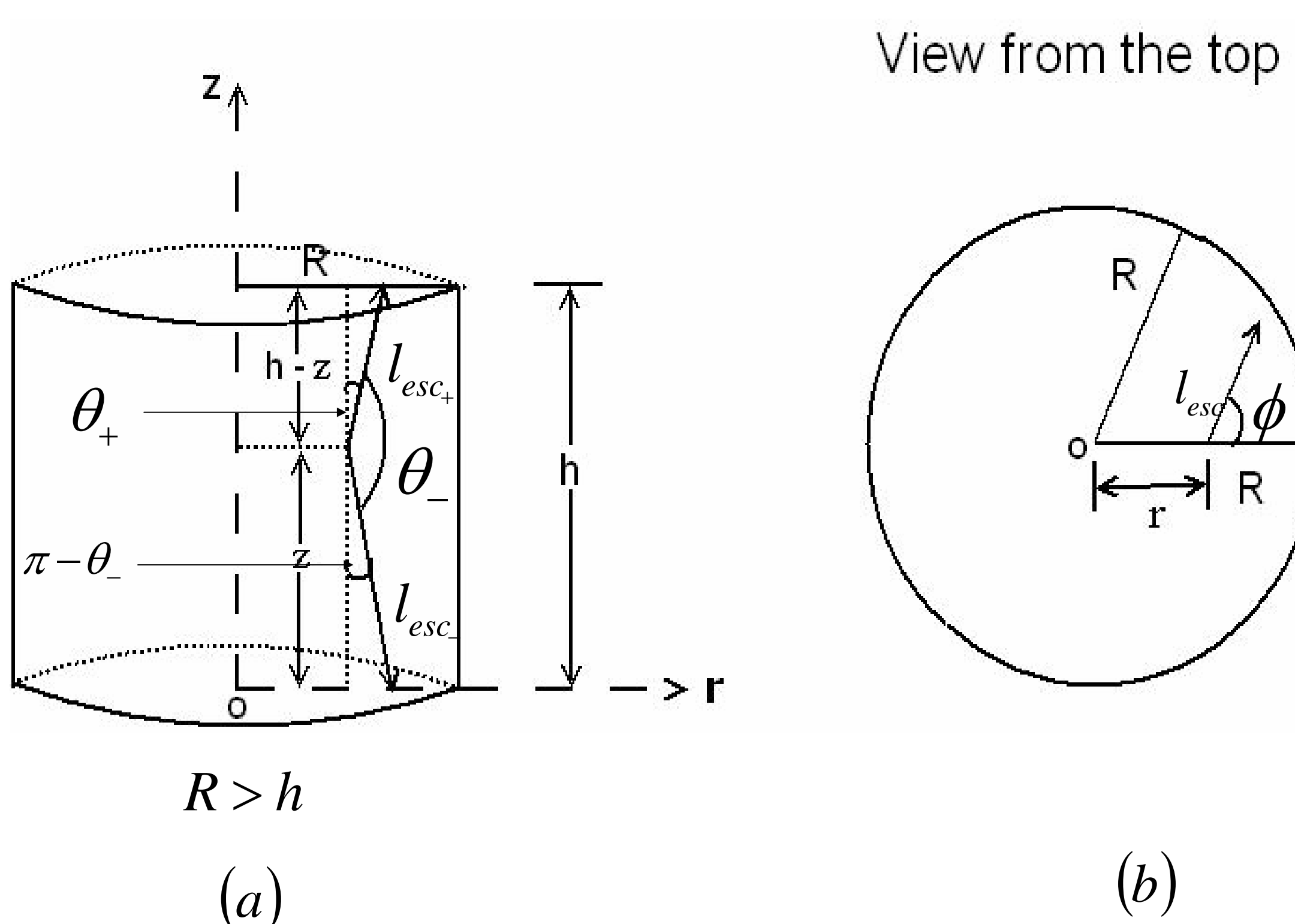

Fig. 2: (a) Depiction of the three possible directions (forward, backward & sideways) of escape for photons from a cylinder. L_{esc+} is the escape length for the forward direction making an θ_+ angle with the axis of the jet (z-axis), & l_{esc-} is that for the backward direction.

(b) Projection of the escape path length on the horizontal surface.

Model Sketch – We consider a cylindrical emission region (Fig. 1) to calculate the spectrum of the emission region in a time-dependent manner. The average photon escape timescale that is needed in these calculations has been obtained independently by considering the three possible directions of escape for photons for a cylindrical geometry [3] and is given by equation 1 (Fig. 2). The inhomogeneity in the photon and particle density throughout the emission region has been considered by dividing the region into multiple zones, each of width h_z and radius R (Fig. 3), same as that of the jet itself. This feature is required to accurately reproduce the observed spectral variability patterns and SED, which in essence, are a combination of various spectra produced in different parts of the region depending on the energies of the available electrons and the density of the photons present in that part of the region. We start with a jet completely devoid of relativistic particles. The 1st population of ultrarelativistic particles is injected by the shocks into the zones closest to the CD in both the directions. As the shock moves through a zone, it accelerates particles at the shock front, which then start to radiate. When the shock enters a new zone, it injects and accelerates the particles there while the injection and acceleration in the previous zone stops and only the cooling continues. The previous zone starts to provide a fraction of its photon density ($dn_{ph, fwd}$ & $dn_{ph, back}$) to its adjacent zones in both the directions while some fraction escapes out of the jet completely and becomes a part of the observed radiation ($dn_{ph, side}$). The spectrum for each zone is calculated individually and then added by taking into account the appropriate light-travel time to generate the SED and light curves in the observer's frame [3].
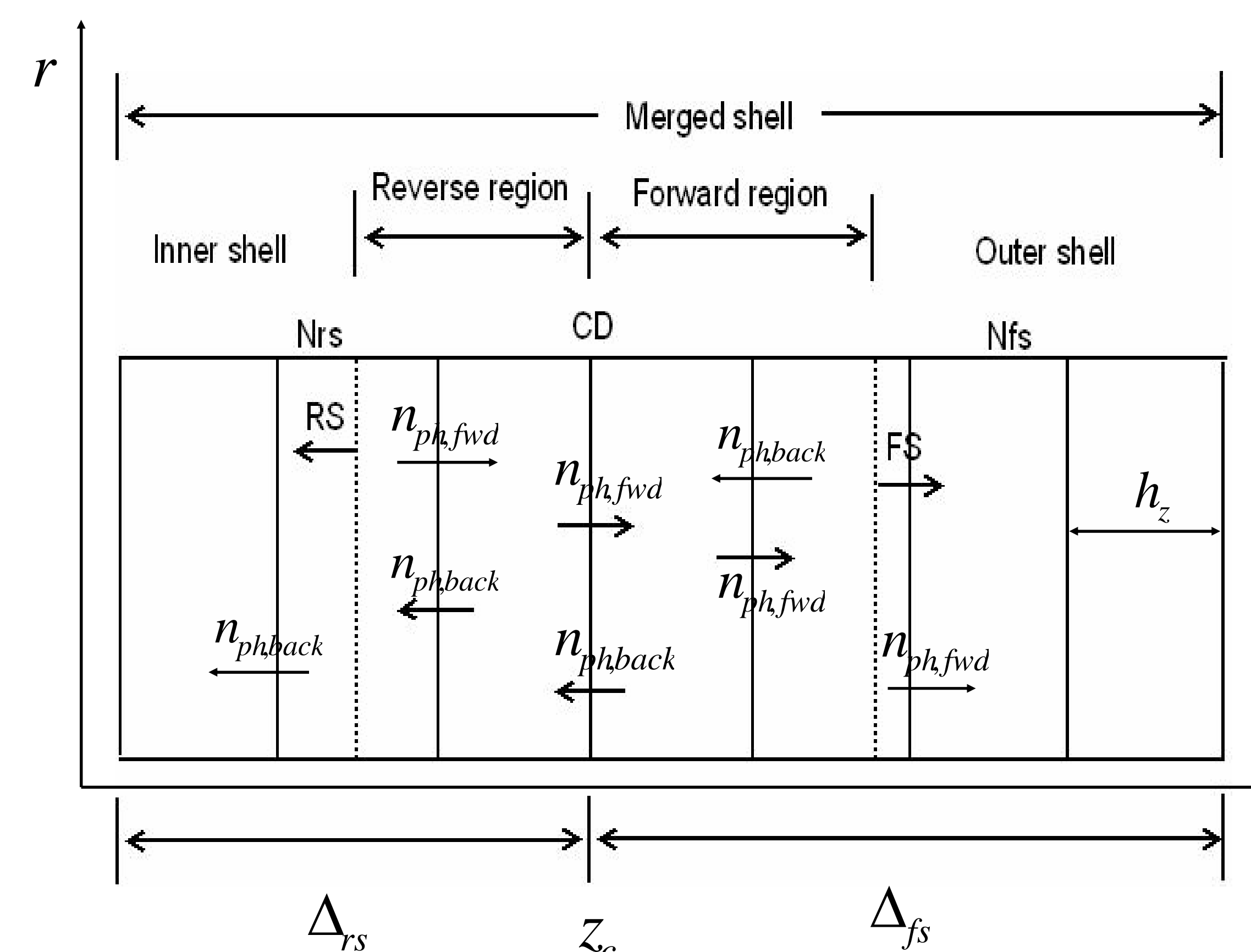

Fig. 3: Schematic of the radiation transfer in between the zones using appropriate photon escape probability functions.

$$\langle t_{ph,esc} \rangle = \frac{1}{4\pi c} \int_0^{2\pi} d\phi \left[\int_{-1}^{\mu_{crit_-}} l_{esc_-}(\theta, \phi; r, z) d\mu + \int_{\mu_{crit_-}}^{\mu_{crit_+}} l_{esc} d\mu + \int_{\mu_{crit_+}}^{+1} l_{esc_+} d\mu \right] \quad (1)$$

$$dn_{ph,fwd} = n_{ph} \frac{dt}{t_{ph,esc}} P_{fwd} \quad (2)$$

where, n_{ph} is the total photon density in a zone at the current time step dt, and P_{fwd} is the escape probability function in the forward direction. Also $P_{back} = P_{fwd}$ by symmetry of the geometry, hence $dn_{ph,back} = dn_{ph,fwd}$

Results – The following two graphs show the simulated SED for the rising (Fig 4) and the decaying (Fig 5) phase of emission for a generic object obtained from a test run of the radiation transfer method. Currently, we are in the process of obtaining the SED for the BL Lac object 3C 66A that includes the effects of shock propagation and radiation transfer method. For this, we assumed a fraction of accelerated electrons to be $\sim 1 \times 10^{-3}$, fraction of the shock's internal energy in the magnetic field to be $\sim 4 \times 10^{-4}$, mass of the outer shell to be $\sim 1 \times 10^{28} g$, $\Gamma_o \approx 10$, & $\Gamma_i \approx 15$. The wind that ejected the two shells had a luminosity of $L_w \approx 1 \times 10^{48}$ erg/s and a duration of $t_w \approx 2 \times 10^5$ s. The emission region was divided into 18 zones with 8 for the RS and 10 for the FS. The radius of the jet, R, was assumed to be $\sim$ 3.59×10^{15} cm with the jet making an angle of 2.4^0 with the observer's line of sight.
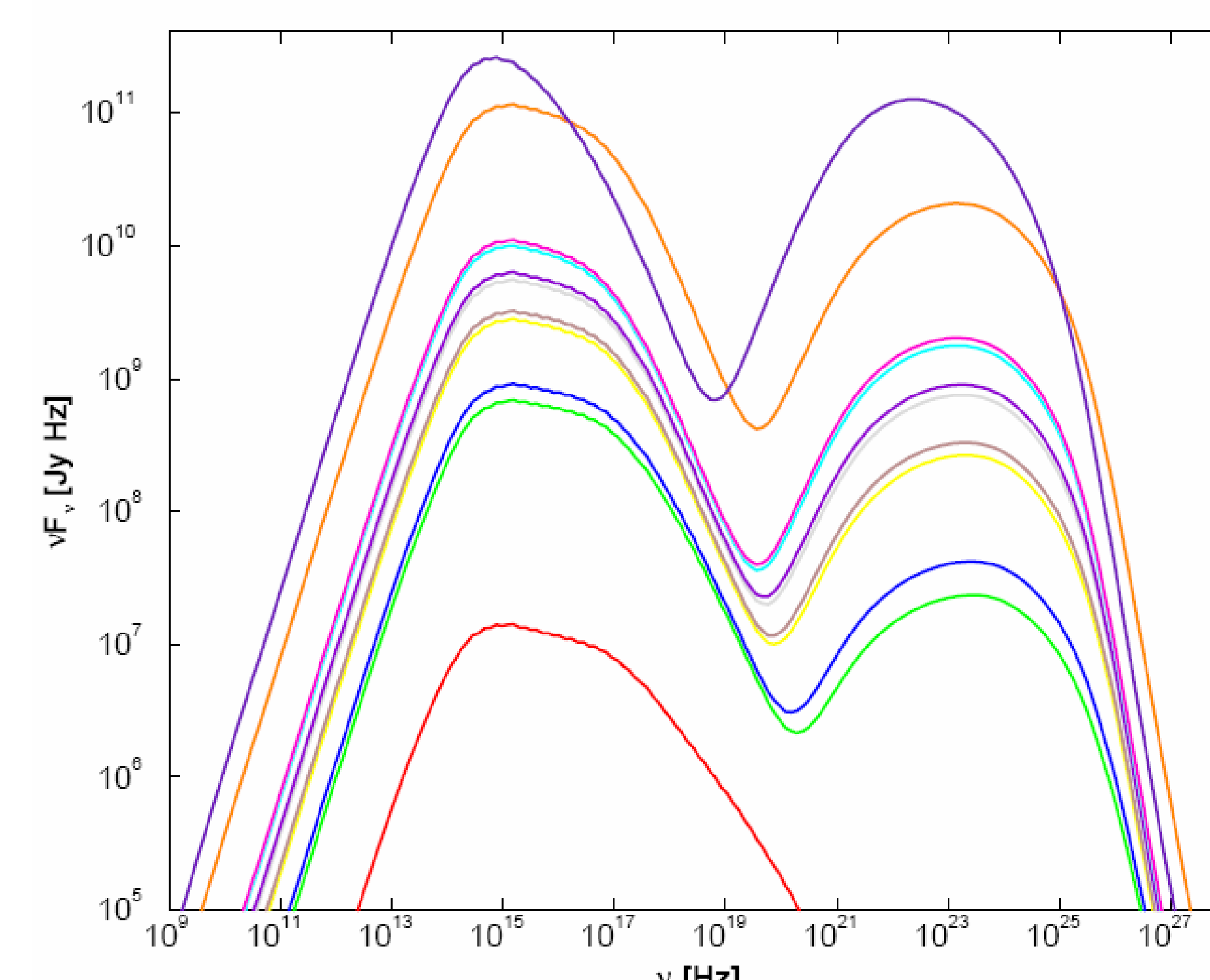

Fig. 4: Simulated SED of a source obtained from the parameters described above. The acceleration is still on in some of the zones and marks the rising phase of emission in a flaring activity.
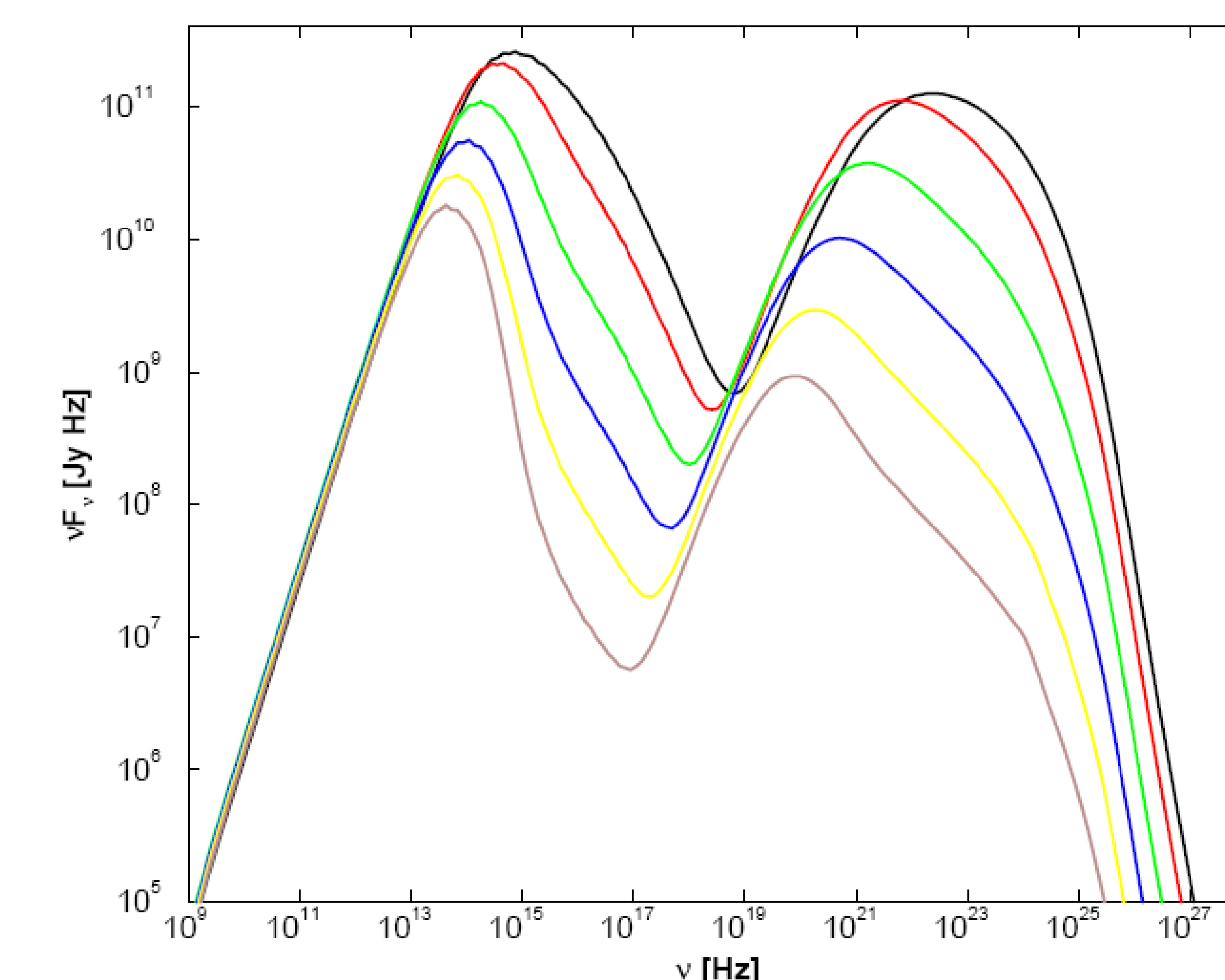

Fig. 5: Simulated SED of a source depicting the decaying phase of emission in a flaring activity. At this time cooling is dominant in all the zones throughout the emission region.

[1] Böttcher, M., & Schlickeiser, R., 1997, A&A, 325, 866, [2] deJager, O. C., & Harding, A. K., 1992, ApJ, 396, 161

[3] Joshi, M., & Böttcher, M., 2008, in preparation, [4] Spada, M., et al., 2001, MNRAS, 325, 1559